Determination of bulk resistivity of $Nd_{9.33}(SiO_4)_6O_2$ single crystal by the DC four-probe method

Susumu Nakayama (Department of Applied Chemistry and Biotechnology, National Institute of Technology (KOSEN), Niihama College, s.nakayama@niihama-nct.ac.jp, Japan)
Mikio Higuchi (Faculty of Engineering, Hokkaido University, hig@eng.hokudai.ac.jp, Japan)
Yasuhiro Nishimura (Honda Research and Development Co., Ltd., yasuhiro_nishimura@n.w.rd.honda.co.jp, Japan)
Yoshikatsu Higuchi (Honda Research and Development Co., Ltd., yoshikatsu_higuchi @n.w.rd.honda.co.jp, Japan)

Abstract

This study aimed to determine the intrinsic bulk resistivity of neodymium silicate $Nd_{9.33}(SiO_4)_6O_2$ single crystals with an apatite-type structure and to clarify the origin of impedance features observed during oxide ion conductivity measurements. The *c*-axis oxide ionic conductivity of neodymium silicate $Nd_{9.33}(SiO_4)_6O_2$ single crystals with an apatite-type crystal structure was measured using AC two-probe and DC four-probe methods. In the Nyquist plot obtained from the AC two-terminal method, an arc was observed at high frequencies, passing through the origin below 350 °C, while a tail appeared at low frequencies. The resistance value corresponding to the intersection with the *Z'* axis on the right-hand (low frequency) side of the arc was found to closely match the resistance measured by the DC four-probe method. This indicates that the arc represents the bulk resistance of the single crystal. As the temperature increased, the arc disappeared, and the tail separated into a new arc and a tail. These arcs and tails were attributed to the ionic transfer resistance on the surface of single crystal and the charge transfer resistance between the single crystal and electrodes. The results also revealed that the AC two-probe method is affected by the resistance of the platinum wires used in measurement, whereas the DC four-probe method provides a more accurate assessment of intrinsic resistivity. The novelty of this work lies in its direct comparison of AC and DC measurement techniques for a single crystal apatite-type oxide, offering new insight into the distinction between bulk and interfacial resistive behaviors and establishing a more reliable approach for evaluating oxide ion conduction in rare-earth silicate materials.

Key words

FZ method, impedance analyzer, complex impedance analysis, arrhenius plots, equivalent circuit

1. Introduction

Fluorite-type oxides such as zirconia, ceria, and bismuth systems, as well as lanthanum gallate oxides with perovskite structures, are well known as oxide ion conductors (Cho et al., 2019; Fu, 2009; Ishihara et al., 2006; Nakayama, 2002; Nakayama et al., 2022). Recently, new hexagonal perovskite-related oxides have also been reported (Fop et al., 2016; Yashima et al., 2021). Most of these materials conduct oxide ions through lattice defects. Conversely, we have developed a rare-earth silicate-based oxide ion conductor with an apatite-type structure that exhibits higher conductivity than zirconia-based oxides in the low-to-medium temperature range (below 500 °C) (Nakayama et al., 1995; 1995; Nakayama and Sakamoto, 1998; Higuchi et al., 2010). The apatite crystal structure of the basic composition $RE_{9.33}(SiO_4)_6O_2$ (RE = rare earth element, La—Dy) is shown in Figure 1 (Okudera et al., 2004; 2005; Nakayama and Sakamoto, 2013). The 2a site along the *c*-axis is occupied by oxygen ions that do not belong to the SiO_4 tetrahedron. Crystal structure analyses and quantum chemical calculations of single crystals have revealed that these oxygen ions at the 2a site play a key role in oxide ion conduction (Fujii et al., 2018). We previously investigated the oxide ion conductivity of $Nd_{9.33}(SiO_4)_6O_2$ single crystals grown by the floating-zone (FZ) method using complex impedance analysis with the AC two-probe method (Nakayama et al., 1999; 2002; 2013; Nakayama and Higuchi, 2001). The results showed that the oxide ion conductivity along the *c*-axis direction is one to two orders of magnitude higher than that perpendicular to the *c*-axis direction, demonstrating a pronounced anisotropy. This finding confirms that oxygen ions at the 2a site along the *c*-axis are strongly involved in ion conduction. In complex impedance analysis using the AC two-probe method, one arc and a tail were observed on the high-frequency side below 350 °C. Above 400 °C, the arc disappeared, and a new arc and tail appeared. We previously hypothesized that these new arc and tail were caused by resistance at the single crystal–electrode interface, although this could not be conclusively determined. Therefore, in this present study, we employed the DC four-terminal method, which eliminates the effects of measurement cable and electrode resistances, allowing measurement of the intrinsic electrical resistance of the crystal itself. The DC four-terminal method accurately measures low resistance values of samples and eliminates the influence of contact resistance due to lead wires. Although adhesion stabilities differ when electrodes are formed on the sample surface by firing or other methods, the DC four-terminal

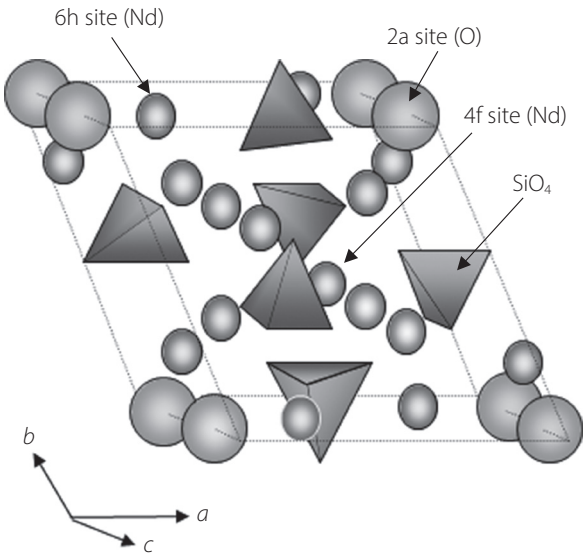

Figure 1: Proposed apatite-type crystal structure for $Nd_{9.33}(SiO_4)_6O_2$

method can eliminate the influence of the electrode material because the contact resistance and polarization effect generated by the two outer electrodes are not included in the measured voltage. Samples (3 × 3 × 20 mm) were cut from $Nd_{9.33}(SiO_4)_6O_2$ single crystals grown by the FZ method, aligned along the c-axis, and used for oxide ion conductivity measurements via the DC four-probe method.

2. Experimental

2.1 Sample preparation

Single crystals were prepared as follows. Nd_2O_3 (Shin-Etsu Chemical Co., Ltd., 99.9%) and SiO_2 (Mitsuwa Chemicals Co., Ltd., Special-grade) were mixed as starting materials in ethanol using a ball mill with a plastic pot. The mixture was dried and then temporarily calcined at 1200 °C in air for 10 h. The resulting powder was milled again, dried, and then pressed into rods using a cold isostatic press at 100 MPa, followed by sintering at 1650 °C in air for 20 h. Single crystals were grown by the FZ method using an infrared furnace (Nichiden Kikai Co. Ltd.: SC-4B) at 1900 °C under N_2 flow, with a growth rate of 5 mm h^{-1} and a rotation speed of 80 rpm. The appearance of the $Nd_{9.33}(SiO_4)_6O_2$ single crystal is shown in Figure 2.

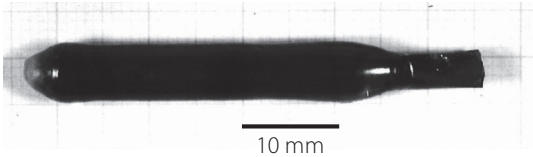

Figure 2: Appearance of the produced $Nd_{9.33}(SiO_4)_6O_2$ single crystal

2.2 Measurements

DC four-probe method measurement samples (size: 3 × 3 × 20 mm) and AC two-probe method measurement samples (size: φ6 mm × t4 mm) were cut and processed from $Nd_{9.33}(SiO_4)_6O_2$ single crystals so that conductivity could be measured parallel to the c-axis. For the DC four-probe measurements, platinum (Pt) paste (Tokuriki Chemical Laboratory Co., Ltd., PT Silvest, No. 8105) was applied to both ends of each sample, and 0.1 mm diameter Pt wires were attached as shown in Figure 3. Another 0.1 mm diameter Pt wire was wound around the center of the sample with an electrode spacing of 10 mm, and the Pt paste was attached. The sample was then baked at 1000 °C to form stable electrodes. Current and voltage values were measured using a multimeter (Advantest Co., TR8050) and a electrometer (ADC Co., 8252), with current controlled by a DC stabilized power supply (Good Will Instrument Co., Ltd., GPS-1830D), in the temperature range of 350 to 800 °C. Resistance values were then calculated. Caution is required even with the DC four-terminal method because thermoelectric power and leakage current can act as noise sources in high-temperature measurements. To reduce the influence of electromotive force, we increased the detection voltage by using a large measurement current. Moreover, a shielded, highly insulated cable was used in the measurement system to reduce the effects of leakage current. For the AC two-probe method, Pt paste was applied to both sides, and 0.05 mm diameter Pt wires were attached and baked at 1000 °C to serve as electrodes. Conductivity was measured between 200 and 800 °C across a frequency range of 100 Hz to 10 MHz using an impedance analyzer (HP 4194A) and determined by complex impedance analysis.

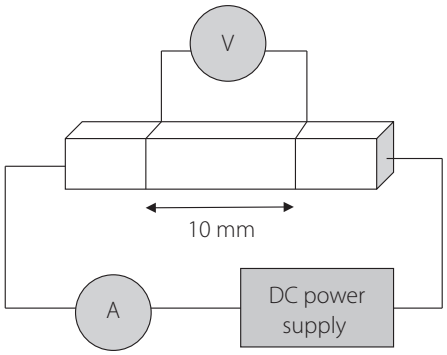

Figure 3: Schematic of the DC four-probe measurement sample and circuit configuration

3. Results and discussion

The Nyquist plots of the samples measured by the AC two-probe method from 200 to 800 °C are summarized in Figure 4 and 5. At 200, 300, and 350 °C, a small arc was observed on the high-frequency side (origin side) and a tail on the low-frequency side (right-hand side) of the arc. At 400 °C, the small arc disappeared, leaving a tail that separated into a larger arc and a tail. The arcs observed below 350 °C are attributed to the bulk resistivity component of $Nd_{9.33}(SiO_4)_6O_2$ single crys-

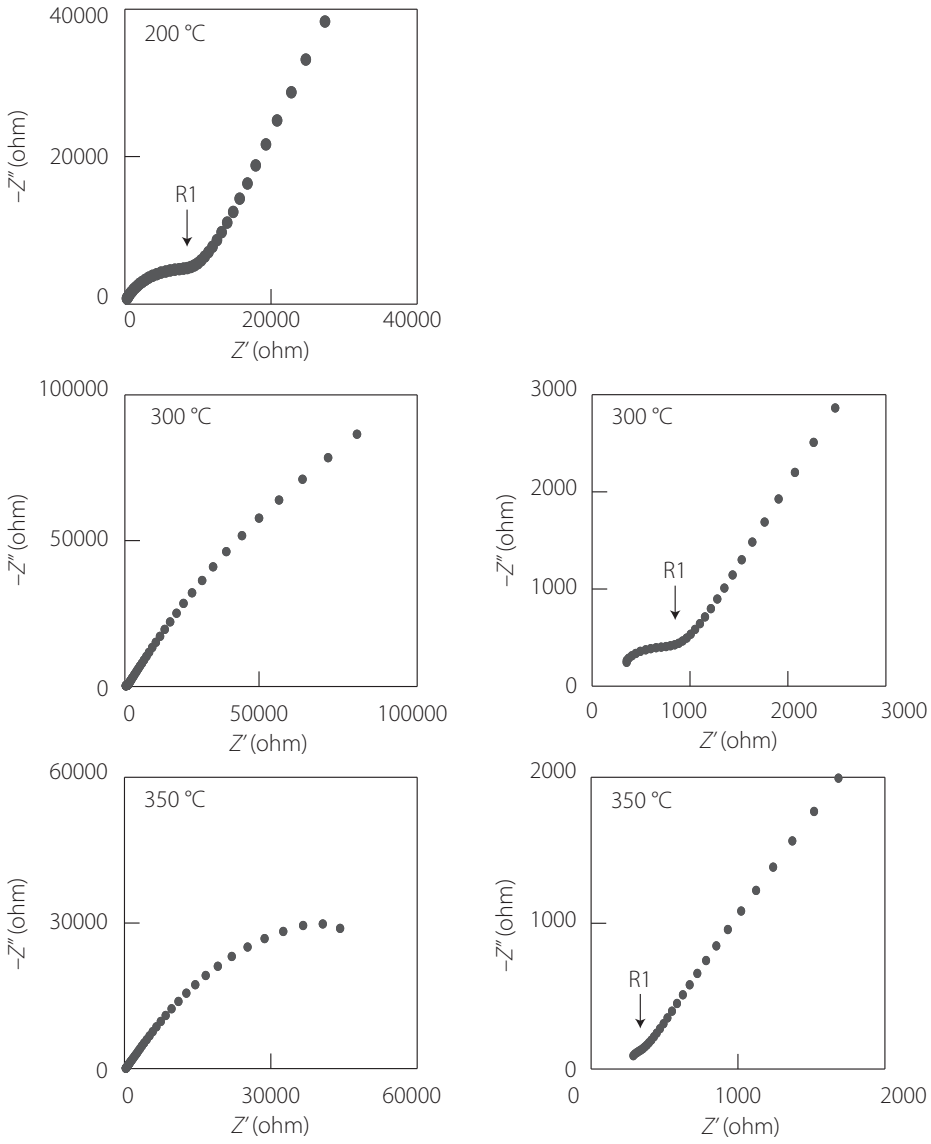

Figure 4: Nyquist plots of the AC two-probe measurement at 200, 300, and 350 °C

tals, while the new arcs observed above 400 °C are attributed to the resistive components at the bulk–electrode interface. Although low-angle grain boundaries can exist even in single crystals, the contribution of such boundaries is expected to be minor. Figure 6 shows Arrhenius plots of the conductivity calculated from resistance values at the intersections (R1 and R2) with the *Z′* axis on the high- and low-frequency sides of the arcs (as indicated by arrows in Figures 4 and 5).

Additionally, the conductivity of the sample measured by the DC four-probe method from 350 to 800 °C is also shown in the Arrhenius plot in Figure 6. Extrapolating the DC four-probe data to temperatures below 350 °C shows good agreement with the conductivity derived from R1, while the conductivity derived from R2 is more than two orders of magnitude lower. Therefore, R1 can be considered representative of the bulk resistivity component of the entire single crystal. The arcs and tails observed above 400 °C are thus attributed to resistive components at the bulk–electrode interface. In a single crystal electrolyte processed to measure conductivity parallel to the *c*-axis, the O^{2-} conduction channel direction is aligned in a uniform direction, facilitating O^{2-} conduction (Figure 7). However, because the Pt electrode is porous, the conducted O^{2-} can reach the Pt electrode directly where the electrolyte and Pt particles meet. Meanwhile, where the electrolyte and Pt particles do not meet, the conducted O^{2-} cannot reach the Pt electrode directly and instead migrates across the electrolyte surface to reach the Pt particles. We speculate that the behavior of the ionic transfer resistance (R_{sele}) on the surface of the electrolyte and the charge transfer resistance (electrode interface resistance, R_{ei}) is observed as arcs and tails above 400 °C. Figure 8 shows an example of an equivalent circuit consisting of bulk (single-crystal) resistance (R_b), R_{sele}, and R_{ei}, as well as a Nyquist diagram for that equivalent circuit.

The conductivity calculated from R1 is slightly lower than that measured by the DC four-probe method at 400 °C and

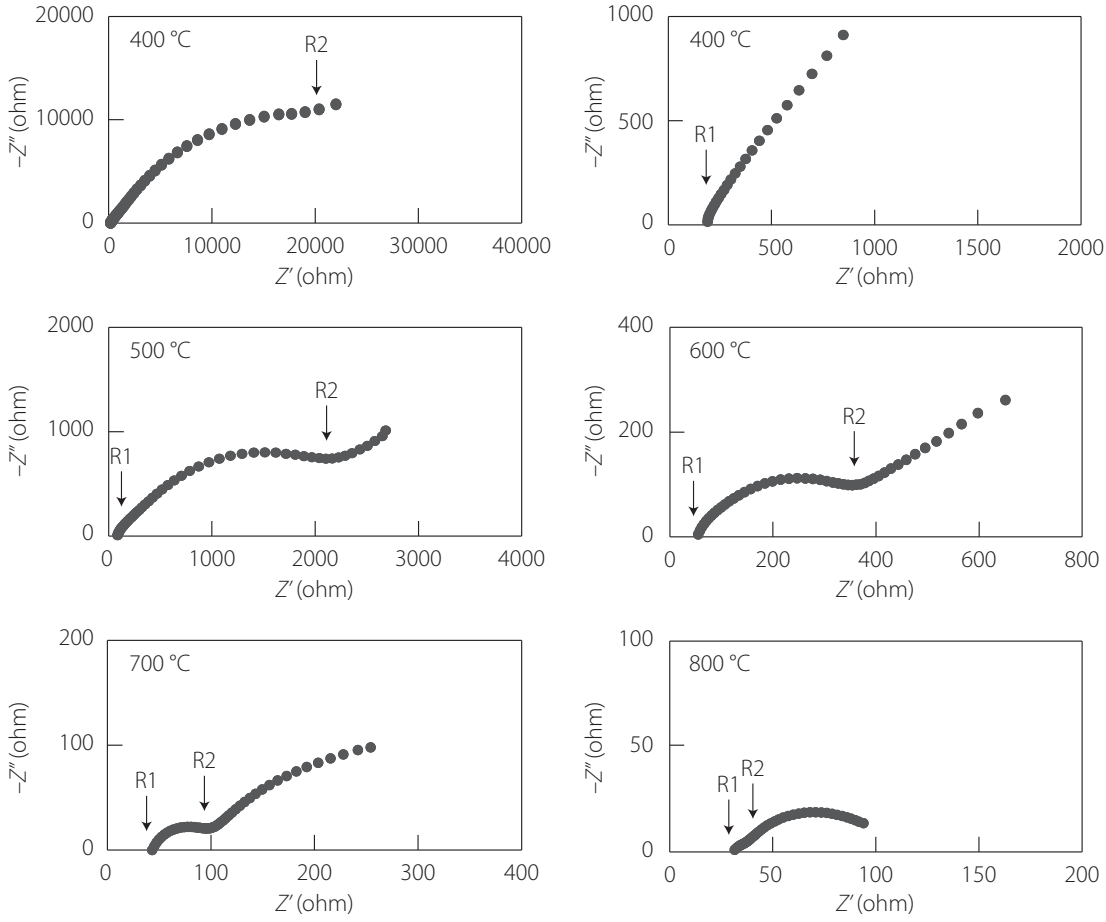

Figure 5: Nyquist plots of the AC two-probe measurement at 400-800 °C

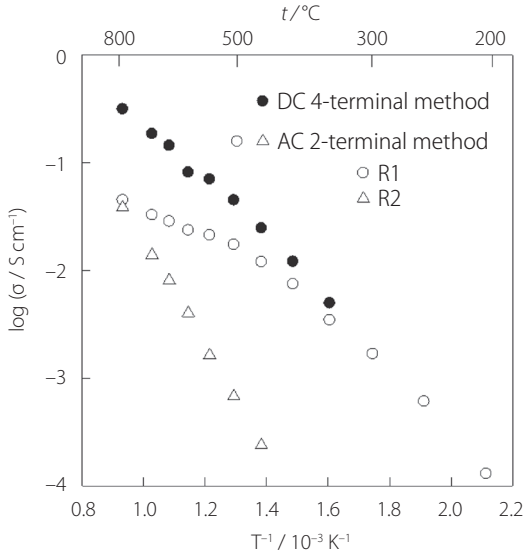

Figure 6: Arrhenius plots of conductivity for the DC four-probe method (closed circles) and AC two-probe method [R1 component in Figures 4 and 5: open circles; R2 component in Figure 4 and 5: open triangles] for $Nd_{9.33}(SiO_4)_6O_2$ single crystals

above, likely due to the resistance of the Pt wires used in the AC measurement. When the measured sample resistance falls below approximately 200 Ω (as above 400 °C), the AC two-probe measurement becomes increasingly influenced by lead resistance. Therefore, for AC two-probe measurements, it is advisable to increase the sample thickness to ensure a measured resistance of at least 200 Ω.

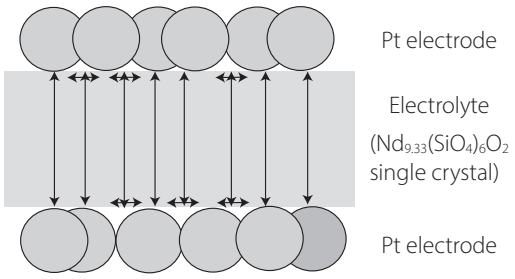

Figure 7: Proposed mechanism of O^{2-} conduction in the electrolyte and electrode (arrows indicate O^{2-} conduction)

4. Conclusion

Neodymium-silicate $Nd_{9.33}(SiO_4)_6O_2$ single crystals with apatite-type crystal structure exhibiting oxide ion conductivity were prepared by the FZ method. Samples oriented along the *c*-axis were cut and processed to enable measurement of oxide ion conductivity. Pt electrodes and Pt wires were attached to each sample, and electrical properties were mea-

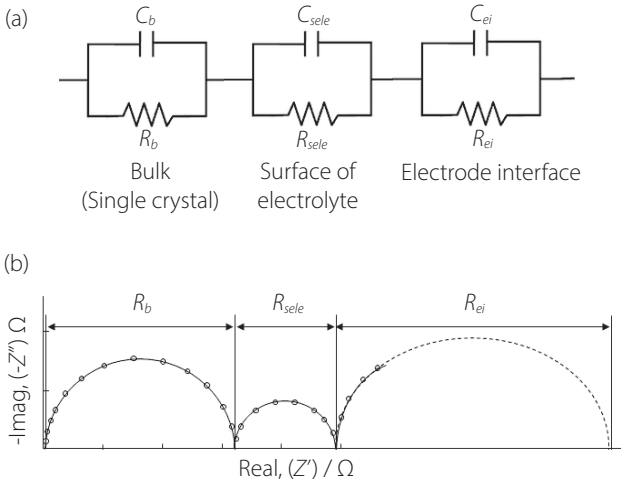

Figure 8: (a) Typical equivalent circuit and (b) Nyquist plot example for the equivalent circuit

sured using both the AC two-probe and DC four-probe methods. In the Nyquist plot obtained from the AC two-probe measurements below 350 °C, a single arc passing through the origin on the high-frequency side and a tail on the low-frequency side were observed. As the temperature increased, the arc disappeared, and the tail separated into a new arc and tail. The resistance value at the intersection with the *Z'* axis on the low-frequency side of the arc observed below 350 °C closely matched the resistance measured by the DC four-probe method, indicating that the arc corresponds to the bulk resistance of the entire single crystal. The arcs and tails observed above 400 °C were attributed to the ionic transfer resistance on the surface of single crystal and the charge transfer resistance between the single crystal and electrodes. It was found that the AC two-probe method is affected by the resistance of the Pt wires used in the measurements. Therefore, to minimize this effect, the sample thickness should be increased such that the measured resistance exceeds 200 Ω. These findings confirm that the DC four-probe method provides a more reliable evaluation of the intrinsic bulk resistivity of $Nd_{9.33}(SiO_4)_6O_2$ single crystals, free from electrode and lead resistance effects. We believe that our study makes a significant contribution to the literature by providing a clear experimental distinction between bulk and interfacial resistive components in apatite-type oxide ion conductors, using $Nd_{9.33}(SiO_4)_6O_2$ single crystals as a model system. By directly comparing AC two-probe and DC four-probe methods, it resolves a long-standing measurement ambiguity in determining true bulk resistivity, thereby improving the reliability of ionic conductivity characterization in single-crystal materials. The findings validate the DC four-probe method as a more accurate technique for intrinsic conductivity assessment and enhance understanding of temperature-dependent interfacial effects that influence impedance behavior.

Acknowledgement

This study was partially supported by a Grant-in-Aid for Scientific Research (KAKENHI, No. JP21560730, JP15K06495, JP19K05009, and JP22K04693) from the Ministry of Education, Culture, Sports, Science, and Technology of Japan, by the Japan Science and Technology Agency JST (Seeds14-025, AS231Z01137C, AS251Z00645M), by the Mazda Foundation (2011KK-ch-072), by the Okura Kazuchika Memorial Foundation (2015-08), and by the Kato foundation for Promotion of Science (KJ-2717). We would also like to thank Editage (www.editage.jp) for English language editing.

References

Cho, C. M., Nunotani, N., and Imanaka, N. (2019). Effect of oxygen vacancies on direct N_2O decomposition over ZrO_2-Y_2O_3 catalysts. *Journal of Asian Ceramic Societies*, Vol. 7, pp. 518-523.

Fop, S., Skakle, J. M. S., McLaughlin, A. C., Connor, P. A., Irvine, J. T. S., Smith, R. I., and Wildman, E. J. (2016). Oxide ion conductivity in the hexagonal perovskite derivative $Ba_3MoNbO_{8.5}$. *Journal of the American Chemical Society*, Vol. 138, pp. 16764-16769.

Fujii, K., Yashima, M., Hibino, K., Shiraiwa, M., Fukuda, K., Nakayama, S., Ishizawa, N., Hanashima, T., and Ohhara, T. (2018). High oxide-ion conductivity by the overbonded channel oxygens in Si-deficient $La_{9.565}(Si_{5.826}\square_{0.174})O_{26}$ apatite without interstitial oxygens. *Journal of Materials Chemistry A*, Vol. 6, pp. 10835-10846.

Fu, Y. P. (2009). Ionic conductivity and mechanical properties of Y_2O_3-doped CeO_2 ceramics synthesis by microwave-induced combustion. *Ceramics International*, Vol. 35, pp. 653-659.

Higuchi, Y., Sugawara, M., Onishi, K., Sakamoto, M., and Nakayama, S. (2010). Oxide ionic conductivities of apatite-type lanthanum silicates and germinates and their possibilities as an electrolyte of lower temperature operating SOFC. *Ceramics International*, Vol. 36, pp. 955-959.

Ishihara, T., Tabuchi, J., Ishikawa, S., Yan, J., Enoki, M., and Matsumoto, H. (2006). Recent progress in $LaGaO_3$ based solid electrolyte for intermediate temperature SOFCs. *Solid State Ionics*, Vol. 177, pp. 1949-1953.

Nakayama, S., Aono, H., and Sadaoka, Y. (1995). Ionic conductivity of $Ln_{10}(SiO_4)_6O_3$ (Ln = La, Nd, Sm, Gd and Dy). *Chemistry Letters*, Vol. 24, pp. 431-432.

Nakayama, S., Kageyama, T., Aono, H., and Sadaoka, Y. (1995). Ionic conductivity of lanthanoid silicates, $Ln_{10}(SiO_4)_6O_3$ (Ln = La, Nd, Sm, Gd, Dy, Y, Ho, Er and Yb). *Journal of Materials Chemistry*, Vol. 5, pp. 1801-1805.

Nakayama, S. and Sakamoto, M. (1998). Electrical properties of new type high oxide ionic conductor $RE_{10}Si_6O_{27}$ (RE = La, Pr, Nd, Sm, Gd, Dy). *Journal of the European Ceramic Society*, Vol. 18, pp. 1413-1418.

Nakayama, S., Sakamoto, M., Higuchi, M., Kodaira, K., Sato, M.,

Kakita, S., Suzuki, T., and Itoh, K. (1999). Oxide ionic conductivity of apatite type $Nd_{9.33}(SiO_4)_6O_{27}$ single crystal. *Journal of the European Ceramic Society*, Vol. 19, pp. 507-510.

Nakayama, S. and Higuchi, M. (2001). Electrical properites of apatite type oxide ionic conductors $RE_{9.33}(SiO_4)_6O_2$ (RE=Pr, Nd and Sm) single crystals. *Journal of Materials Science Letters*, Vol. 20, pp. 913-915.

Nakayama, S. (2002). Electrical properties of $(Bi_2O_3)_{0.75}(RE_2O_3)_{0.25}$ ceramics (RE= Dy, Y, Ho, Er and Yb). *Ceramics Internatinal*, Vol. 28, pp. 907-910.

Nakayama, S., Higuchi, M., and Uematsu, K. (2002). Relationship between conductivities and compositions determined by EPMA for apatite-type $Nd_x(SiO_4)_6O_{1.5x-12}$ single crystals. *Nippon Kagaku Kaishi*, Vol. 2002, No. 2, pp. 243-245. (in Japanese)

Nakayama, S., Ikesue, A., Higuchi, Y., Sugawara, M., and Sakamoto, M. (2013). Growth of single-crystals of apatite-type oxide ionic conductor from sintered ceramics by a seeding method. *Journal of the European Ceramic Society*, Vol. 33, pp. 207-210.

Nakayama, S. and Sakamoto, M. (2013). Preparation of apatite-type $La_{9.33}Ge_6O_{26}$ single-crystal from sintered ceramics by a seeding method and its oxide ionic conduction. *Solid State Ionics*, Vol. 253, pp. 47-52.

Nakayama, S., Tokunaga, R., Takata, M., Kondo, S., and Nakajima, Y. (2021). Crystal phase, electrical properties, and solid oxide fuel cell electrolyte application of scandia-stabilized zirconia doped with rare earth elements. *Open Ceramics*, Vol. 6, 100136.

Okudera, H., Yoshiasa, A., Masubuchi, Y., Higuchi, M., and Kikkawa, S. (2004). Temperature dependence of structural parameters in oxide-ion-conducting $Nd_{9.33}(SiO_4)_6O_2$: single crystal X-ray studies from 295 to 900K. *Journal of Solid State Chemistry*, Vol. 177, pp. 4451-4458.

Okudera, H., Masubuchi, Y., Kikkawa, S., and Yoshiasa, A. (2005). Structure of oxide ion-conducting lanthanum oxyapatite, $La_{9.33}(SiO_4)_6O_2$. *Solid State Ionics*, Vol. 176, pp. 1473-1478.

Yashima, M., Tsujiguchi, T., Sakuda, Y., Yasui, Y., Zhou, Y., Fujii, K., Torii, S., Kamiyama, T., and Skinner, S.J. (2021). High oxide-ion conductivity through the interstitial oxygen site in $Ba_7Nb_4MoO_{20}$-based hexagonal perovskite related oxides. *Nature Communications*, Vol. 12, 556.

Received: October 28, 2025
Accepted: December 2, 2025
Published: December 25, 2025

https://doi.org/10.11425/sst.14.175